

# Fullerene-Functionalized Monolayer-Protected Silver Clusters: $[\text{Ag}_{29}(\text{BDT})_{12}(\text{C}_{60})_n]^{3-}$ ( $n = 1-9$ )

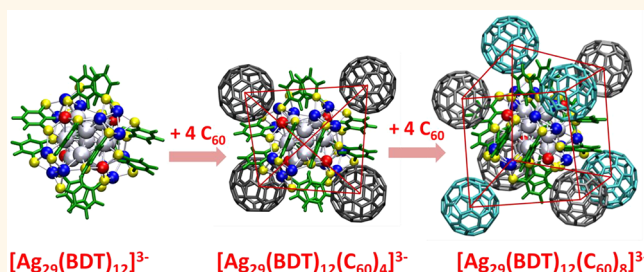
Papri Chakraborty, Abhijit Nag, Ganesan Paramasivam, Ganapati Natarajan, and Thalappil Pradeep\*<sup>1b</sup>

DST Unit of Nanoscience (DST UNS) and Thematic Unit of Excellence (TUE), Department of Chemistry, Indian Institute of Technology Madras, Chennai 600 036, India

## Supporting Information

**ABSTRACT:** We report the formation of supramolecular adducts between monolayer-protected noble metal nano-clusters and fullerenes, specifically focusing on a well-known silver cluster,  $[\text{Ag}_{29}(\text{BDT})_{12}]^{3-}$ , where BDT is 1,3-benzenedithiol. We demonstrate that  $\text{C}_{60}$  molecules link with the cluster at specific locations and protect the fragile cluster core, enhancing the stability of the cluster. A combination of studies including UV–vis, high-resolution electrospray ionization mass spectrometry, collision-induced dissociation, and nuclear magnetic resonance spectroscopy revealed structural details of the fullerene-functionalized clusters,  $[\text{Ag}_{29}(\text{BDT})_{12}(\text{C}_{60})_n]^{3-}$  ( $n = 1-9$ ). Density functional theory (DFT) calculations and molecular docking simulations affirm compatibility between the cluster and  $\text{C}_{60}$ , resulting in its attachment at specific positions on the surface of the cluster, stabilized mainly by  $\pi$ – $\pi$  and van der Waals interactions. The structures have also been confirmed from ion mobility mass spectrometry by comparing the experimental collision cross sections (CCSs) with the theoretical CCSs of the DFT-optimized structures. The gradual evolution of the structures with an increase in the number of fullerene attachments to the cluster has been investigated. Whereas the structure for  $n = 4$  is tetrahedral, that of  $n = 8$  is a distorted cube with a cluster at the center and fullerenes at the vertices. Another fullerene,  $\text{C}_{70}$ , also exhibited similar behavior. Modified clusters are expected to show interesting properties.

**KEYWORDS:** monolayer-protected clusters, fullerenes, supramolecular functionalization, hybrid nanostructures, host–guest chemistry, mass spectrometry, ion mobility



Study of atomically precise clusters of noble metals, covering over 100 well-defined molecular systems, is an expanding discipline.<sup>1–4</sup> Among these, the clusters investigated thoroughly include  $\text{Au}_{25}(\text{SR})_{18}$ ,<sup>5,6</sup>  $\text{Au}_{38}(\text{SR})_{24}$ ,<sup>7</sup>  $\text{Au}_{102}(\text{SR})_{44}$ ,<sup>8</sup>  $\text{Ag}_{25}(\text{SR})_{18}$ ,<sup>9</sup>  $\text{Ag}_{44}(\text{SR})_{30}$ ,<sup>10,11</sup>  $\text{Ag}_{29}(\text{S}_2\text{R})_{12}$ ,<sup>12</sup> etc. While single-crystal X-ray diffraction has been used to solve their crystal structures, mass spectrometric techniques, especially electrospray ionization (ESI) and matrix-assisted laser desorption ionization (MALDI), have been the principal tools to understand their molecular composition.<sup>13,14</sup> These clusters show specific signatures in their optical absorption and luminescence spectra which depend strongly on the ligand–metal interface.<sup>15,16</sup>

Several ligand-protected noble metal clusters of the type  $\text{Au}_{25}(\text{SR})_{18}$ ,  $\text{Ag}_{25}(\text{SR})_{18}$ ,  $\text{Ag}_{29}(\text{S}_2\text{R})_{12}$ , etc. are negatively charged and exist with counterions in their crystal lattice. The inherent charge and electron density of the clusters are typically distributed at the ligand–metal interface. In addition, appropriate molecular dimensions of the system and orientation of the ligands on the cluster surface can induce specific host–guest interactions.<sup>17</sup> These suggest a possibility of exploring supramolecular chemistry of monolayer-protected clusters. An important chemical probe to utilize such properties

of the clusters is fullerenes due to their tendency to form self-assembled structures.<sup>18–20</sup>  $\text{C}_{60}$  is known to form supramolecular complexes with a wide variety of molecules like rotaxanes, catenanes,<sup>21</sup> calixarenes,<sup>22</sup> cyclodextrins,<sup>23</sup> cucurbiturils,<sup>24</sup> crown ethers,<sup>25</sup> and porphyrins.<sup>26–28</sup> Such complexes are mainly stabilized by  $\pi$ – $\pi$ , C–H– $\pi$ , or van der Waals (vdW) interactions.<sup>29,30</sup>

Fullerenes, due to their large number of lowest unoccupied molecular orbitals, which are typically degenerate, can also accept multiple electrons, leading to polyanionic species. Compounds such as  $\text{K}_n\text{C}_{60}$  ( $n = 1-6$ )<sup>31,32</sup> are well-known for interesting properties such as metallicity and superconductivity.<sup>33–35</sup> In addition to complete electron transfer leading to  $(\text{C}_{60})_n^-$ ,  $\text{C}_{60}$  is also known to form partial charge transfer complexes with donors such as tetrathiafulvalene,<sup>36,37</sup> dithia-diazafulvalene,<sup>38</sup> tetraphenyldipyrynylidene, and metallo-cenes.<sup>39</sup> The extent of charge transfer is also limited by the close approach of the molecules and steric factors affecting the overlap of molecular orbitals.<sup>40</sup>

Received: November 1, 2017

Accepted: February 14, 2018

Published: February 14, 2018

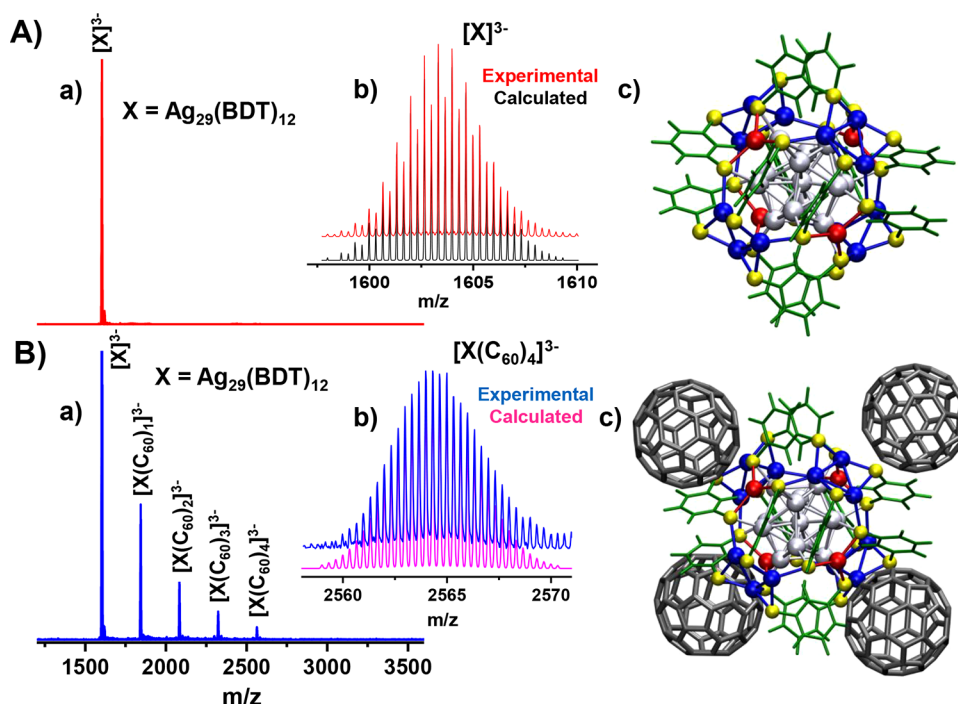


**Figure 1.** (A) (a) Full range ESI MS, (b) experimental and calculated isotope patterns, and (c) DFT-optimized structure of the  $[Ag_{29}(BDT)_{12}]^{3-}$  cluster. (B) (a) ESI MS of  $[Ag_{29}(BDT)_{12}(C_{60})_n]^{3-}$  ( $n = 1-4$ ) complexes, (b) experimental and calculated isotope patterns of  $[Ag_{29}(BDT)_{12}(C_{60})_4]^{3-}$ , and (c) schematic of the possible structure of  $[Ag_{29}(BDT)_{12}(C_{60})_4]^{3-}$ . Color codes for the atoms in the inset pictures: yellow, S atoms; gray, Ag atoms of the icosahedral ( $Ag_{13}$ ) core and the bonds connecting them; blue, 12 Ag atoms of the trigonal planes in the exterior shell and the bonds connecting them to the S atoms of the  $Ag_3S_3$  motifs; red, four Ag atoms face-capping the core at four tetrahedral positions of  $[Ag_{29}(BDT)_{12}]^{3-}$  and the bonds connecting each of these Ag atoms to the neighboring three S atoms; green, BDT ligands; black,  $C_{60}$  molecules.

The foregoing suggests the possibility to create intercluster compounds of monolayer-protected clusters with fullerenes. In view of the specific geometry of the clusters, accessibility of  $C_{60}$  to the cluster surface may be limited, allowing specific composition of the adducts to be feasible. Considering the easiness of accessibility of the metal cluster surface, we chose  $[Ag_{29}(BDT)_{12}]^{3-12}$  as the cluster of choice for these investigations, which confirmed our conjecture. Our studies involved mass spectrometry extensively along with critical inputs from NMR spectroscopy and computational studies. The cluster–fullerene complexes,  $[Ag_{29}(BDT)_{12}(C_{60})_n]^{3-}$  ( $n = 1-4$ ), were mainly stabilized by vdW forces and  $\pi$ – $\pi$  interactions of the fullerenes with the benzene rings of the BDT ligands of the cluster, and they can be characterized completely in the gaseous and solution phases. We further show that, by controlling the conditions, the entire surface of the cluster can be functionalized by fullerenes, which forms close-packed structures. Density functional theory (DFT) calculations and molecular docking simulations were used to elucidate the structure of the fullerene-protected clusters,  $[Ag_{29}(BDT)_{12}(C_{60})_n]^{3-}$  ( $n = 1-4, 8, \text{ and } 9$ ). Studies suggest the occupation of tetrahedral sites of the cluster by  $C_{60}$ . When these positions were occupied as in the case of  $[Ag_{29}(BDT)_{12}(TPP)_4]^{3-}$ , where TPP is triphenylphosphine,  $C_{60}$  substitution did not occur, supporting the structural predictions. Interaction of the cluster with another fullerene,  $C_{70}$ , is also presented in this study.

## RESULTS AND DISCUSSION

$[Ag_{29}(BDT)_{12}]^{3-}$  cluster<sup>12</sup> was synthesized following a reported protocol with slight modifications, as described in the

Experimental section and characterized using optical absorption and ESI MS studies (Figure S1). The structure consists of a  $Ag_{13}$  icosahedral core, which is further capped by 12 Ag atoms of the exterior shell. These 12 Ag atoms form four tetrahedrally oriented trigonal prisms, and another four Ag atoms face-cap the 13 atom core at four tetrahedral positions. This tetrahedral orientation is shown in Figure 1A(c), where the four Ag atoms resemble the vertices (V) of a tetrahedron and four trigonal planes formed by the 12 Ag atoms lie over the faces (F) of the tetrahedron (see Figure S2 for more details). We follow this notation throughout the paper. Additional structural insight may be derived from a three-dimensional view (Video V1 in the Supporting Information).

**Characterization of  $[Ag_{29}(BDT)_{12}(C_{60})_n]^{3-}$  ( $n = 1-4$ ) Complexes.** Complexes of  $C_{60}$  with the cluster,  $[Ag_{29}(BDT)_{12}]^{3-}$ , were obtained by adding a solution of  $C_{60}$  in toluene to the solution of the cluster in DMF in various molar ratios. In Figure 1A, panel (a) shows the ESI MS of the synthesized  $[Ag_{29}(BDT)_{12}]^{3-}$  cluster, which exhibits the molecular ion peak around  $m/z$  1603. Experimental and calculated isotope patterns are shown in (b). DFT-optimized structure based on the crystal structure of the cluster<sup>12</sup> is in (c). Reactivity of  $C_{60}$  with  $[Ag_{29}(BDT)_{12}]^{3-}$  was studied by ESI MS, as shown in Figure 1B. A series of peaks appeared upon addition of  $C_{60}$ . Expansion of these peaks showed that the separation between each of the peaks present in the isotope pattern was 0.33, which corresponded to a charge state of  $3^-$  for the addition complexes, as well. The peaks were separated by  $m/z$  240, which corresponded to the addition of  $C_{60}$  (mass of  $C_{60}$  is  $240 \times 3 = 720$ ). The number of  $C_{60}$  additions increased with increase in the concentration of  $C_{60}$  added to the cluster

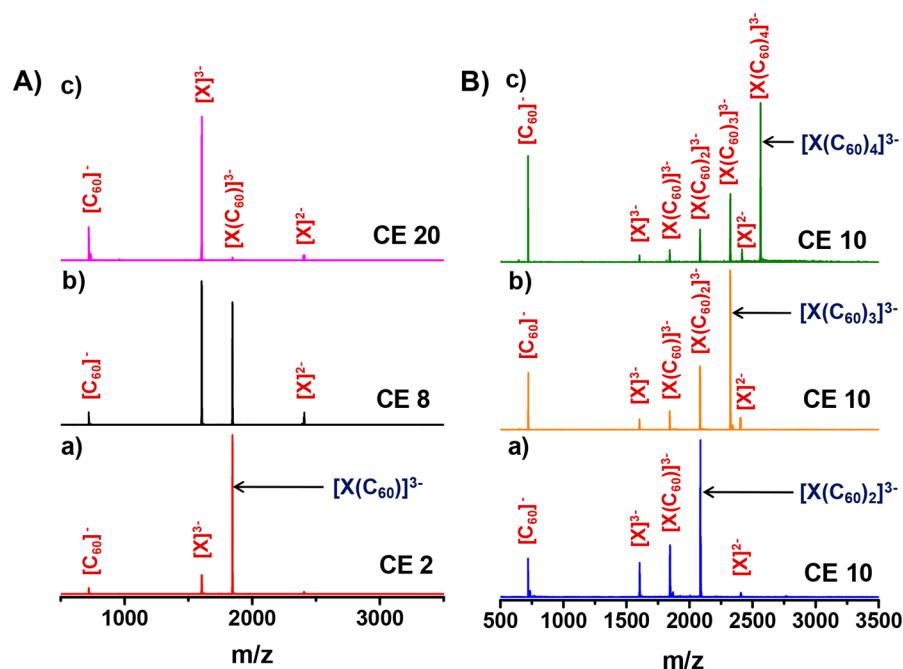
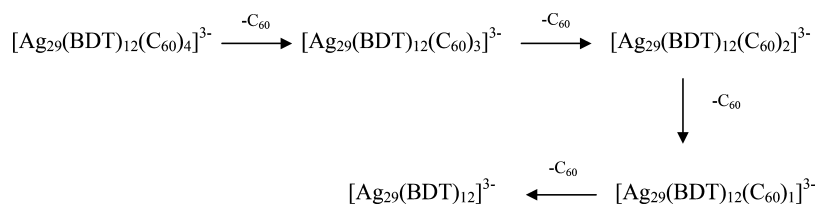


Figure 2. (A) CID study on  $[X(C_{60})]^{3-}$  at increasing collision energies (CE in instrumental units) of 2 (a), 8 (b), and 20 (c). (B) CID spectrum of  $[X(C_{60})_n]^{3-}$  ( $n = 2-4$ ) are shown in (a-c), respectively, at CE 10,  $X = Ag_{29}(BDT)_{12}$ .

#### Scheme 1. Fragmentation Pathway of $[Ag_{29}(BDT)_{12}(C_{60})_n]^{3-}$ ( $n = 1-4$ ) Complexes



(Figure S3). At an optimum concentration, where the cluster/fullerene molar ratio was 1:4, up to four  $C_{60}$  additions were observed in ESI MS, as shown in Figure 1B(a). The experimentally obtained isotope patterns were matched with the calculated patterns to further confirm their composition. The isotope patterns of one of the complexes,  $[Ag_{29}(BDT)_{12}(C_{60})_4]^{3-}$ , is shown in (b), and the rest are included in the Supporting Information (Figure S4). From a comparison of the absorption spectra of the adducts with that of the cluster and  $C_{60}$ , it appeared that the absorption features of the adducts were mainly additive with slight changes in the absorbance when compared to their added spectrum (Figure S5). There was an increase in the absorbance of the  $C_{60}$  features in their adducts. Though such changes reflected the possibility of some electronic coupling between the cluster and the fullerenes, it was very small, and the interactions were mainly supramolecular in nature.<sup>29,41</sup>

As the parent  $[Ag_{29}(BDT)_{12}]^{3-}$  clusters were synthesized without the co-protection from the TPP ligands, they were stable only for a few hours.<sup>12</sup> However, functionalization with  $C_{60}$  increased the stability of the cluster. The complexes were stable for more than a week (Figure S6).  $C_{60}$  molecules act as secondary ligands protecting the cluster core. The dithiol ligands of the cluster are bound in such a fashion that, surrounding each tetrahedral vertex position of the cluster, benzene rings of three of the BDT ligands are oriented in a way that can enhance the stabilization of a  $C_{60}$  molecule at those

positions by  $\pi$ - $\pi$  interaction and also by C-H- $\pi$  contacts at the ligand periphery. Also, appropriate geometry and increased accessibility of the cluster surface allows  $C_{60}$  molecules to come in close proximity of the cluster, which reveals the importance of the structure in the formation of such complexes. A schematic of the most plausible structure of  $[Ag_{29}(BDT)_{12}(C_{60})_4]^{3-}$  is shown in Figure 1B(c).

The binding of fullerenes to the cluster was further supported by elemental analysis. The Ag/S/C atomic ratio for the fullerene adducts of the cluster as obtained from scanning electron microscopy (SEM)/energy-dispersive X-ray spectroscopy (EDS) was 1:0.82:9.07 (expected atomic ratio in  $[Ag_{29}(BDT)_{12}(C_{60})_4]^{3-}$  is 1:0.83:10.76) (Figure S7A). In the case of only the cluster, SEM/EDS showed a Ag/S/C atomic ratio of 1:0.80:2.26 (expected atomic ratio in  $[Ag_{29}(BDT)_{12}]^{3-}$  is 1:0.83:2.48) (Figure S7B). The percentage of C in the composite material ( $[Ag_{29}(BDT)_{12}(C_{60})_n]^{3-}$  ( $n = 1-4$ )) increased in comparison to the parent cluster ( $[Ag_{29}(BDT)_{12}]^{3-}$ ), and the atomic ratios were in close agreement with the expected atomic ratios from their molecular formulas. The slightly reduced carbon content in the experiment in comparison to the theoretical value in  $[Ag_{29}(BDT)_{12}(C_{60})_4]^{3-}$  was due to the various  $C_{60}$  adducts ( $n = 1-4$ ) possible in the sample.

**Collision-Induced Dissociation (CID) Studies.** We carried out CID studies on each of these complexes,  $[Ag_{29}(BDT)_{12}(C_{60})_n]^{3-}$  ( $n = 1-4$ ) (Figure 2) to gain further

insight into the structure and nature of interactions.<sup>42,43</sup> For the simplest case of one C<sub>60</sub> addition to the cluster, [Ag<sub>29</sub>(BDT)<sub>12</sub>(C<sub>60</sub>)<sup>3-</sup>, upon increasing the collision energy (CE, instrumental unit), C<sub>60</sub> was lost from the cluster, and [Ag<sub>29</sub>(BDT)<sub>12</sub>]<sup>3-</sup> and C<sub>60</sub><sup>-</sup> were detected (Figure 2A). Apart from that, [Ag<sub>29</sub>(BDT)<sub>12</sub>]<sup>2-</sup> was also detected in very low intensities. The dissociation pattern was similar for the other higher complexes also, which showed sequential loss of C<sub>60</sub> molecules with an increase in CE. In Figure 2B, we have presented a CID spectra for [Ag<sub>29</sub>(BDT)<sub>12</sub>(C<sub>60</sub>)<sub>n</sub>]<sup>3-</sup> (*n* = 2–4) at CE 10. A systematic energy-dependent study is included in the Supporting Information (Figure S8). CID suggests that the probable fragmentation pathway of these complexes is by the loss of neutral C<sub>60</sub> molecules, as shown in Scheme 1.

Some contribution of charge separation during fragmentation leads to the formation of [Ag<sub>29</sub>(BDT)<sub>12</sub>]<sup>2-</sup> and C<sub>60</sub><sup>-</sup>. Even without any applied collision energy, some extent of dissociation was observed in all cases. Such a behavior was also reflected in the intensity pattern of the complexes observed in ESI MS, as shown in Figure 1B(a). Fragmentation during ionization thus complicates the exact quantification of the proportion of each of these complexes in solution.

**NMR Study.** NMR experiments were performed in order to evaluate the interaction between the cluster and the C<sub>60</sub> molecules (Figure 3). The <sup>13</sup>C NMR was taken in a binary

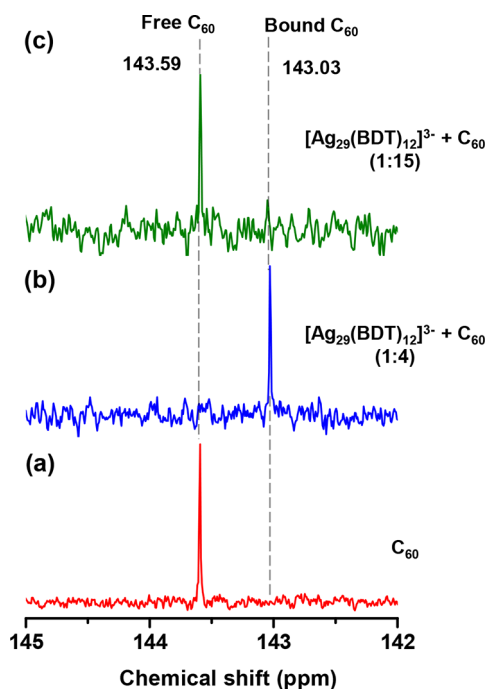


**Figure 3.** NMR of (a) C<sub>60</sub> showing a peak at 143.59 ppm, (b) adducts at a cluster/fullerene molar ratio of 1:4 showing a peak at 143.03 ppm for the C<sub>60</sub> molecules in the bound state, and (c) adducts at an excess concentration of C<sub>60</sub> (cluster/fullerene molar ratio of 1:15) showing a predominant peak for free C<sub>60</sub> (143.59 ppm) and a less intense peak for bound C<sub>60</sub> (143.03 ppm).

solvent mixture, DMF/toluene (2:1 v/v). The peak for C<sub>60</sub> was observed around 143.59 ppm (Figure 3a). NMR for the complexes was taken at a cluster/fullerene molar ratio of 1:4. Upon addition of the cluster, with no change in solvent composition, there was an upfield shift to 143.03 ppm (Figure 3b). Thus, when compared to the NMR of C<sub>60</sub> in the same

solvents, in the presence of the cluster, an upfield shift of about 0.56 ppm was seen, which can be attributed to the shielding effect of the  $\pi$ -conjugated system of C<sub>60</sub>.<sup>44–46</sup> This revealed that the electron density of C<sub>60</sub> was slightly increased in the presence of the clusters. Though at the 1:4 molar ratio, a single peak was observed for the C<sub>60</sub> molecules in their bound state, NMR of the adducts in the presence of excess fullerene (molar ratio of 1:15) showed a predominant peak for free C<sub>60</sub> and a low intense peak for bound C<sub>60</sub> (Figure 3c).

#### Formation of [Ag<sub>29</sub>(BDT)<sub>12</sub>(C<sub>60</sub>)<sub>n</sub>]<sup>3-</sup> (*n* > 4) Complexes.

Upon reaction of the cluster with an excess concentration of C<sub>60</sub> (cluster/fullerene molar ratio was 1:15), a higher number of attachments (*n* = 1–12) were observed in ESI MS, though at low intensities (Figure S9). This suggests that the cluster can become highly protected by the C<sub>60</sub> molecules so that the entire surface of the cluster is covered by fullerenes.

**Computational Modeling To Understand the Structures of [Ag<sub>29</sub>(BDT)<sub>12</sub>(C<sub>60</sub>)<sub>n</sub>]<sup>3-</sup> (*n* = 1–4, 8, and 9).** The interaction of the fullerenes, C<sub>60</sub> and C<sub>70</sub>, on the surface of [Ag<sub>29</sub>(BDT)<sub>12</sub>]<sup>3-</sup> cluster was computationally studied using DFT with the projector-augmented wave method as implemented in GPAW<sup>47,48</sup> using the Perdew–Burke–Ernzerhof (PBE) functional<sup>49</sup> and DZP (double- $\zeta$  plus polarization) LCAO basis set. We searched structures in DFT by attaching C<sub>60</sub>/C<sub>70</sub> at possible locations (tetrahedral vertex sites) on the cluster surface considering geometrical compatibility and stabilization by the supramolecular forces. The orientation of fullerenes at the cluster surface (to facilitate interaction with hexagonal (C<sub>6</sub>) face, pentagonal (C<sub>5</sub>) face, 6–6 bond, and 6–5 bond) was also varied to search the lowest energy conformers of the adducts. Complete computational details are included in the Supporting Information.

**Structure of [Ag<sub>29</sub>(BDT)<sub>12</sub>(C<sub>60</sub>)<sup>3-</sup>. DFT Calculations.** The DFT-optimized geometry of the lowest energy isomer of [Ag<sub>29</sub>(BDT)<sub>12</sub>(C<sub>60</sub>)<sup>3-</sup> with C<sub>60</sub> at the vertex position of the cluster, with a 6–5 bond of C<sub>60</sub> closest to the vertex Ag atom, is shown in Figure 4. The orientation of C<sub>60</sub> having a 6–5 bond closest to the metal center is known in the case of several C<sub>60</sub>/metalloporphyrin complexes.<sup>50</sup> However, the energy difference between the different calculated isomers of [Ag<sub>29</sub>(BDT)<sub>12</sub>(C<sub>60</sub>)<sup>3-</sup> obtained by rotation of C<sub>60</sub> at the vertex site of the cluster was very narrow and was in the range of 0.044 eV (Table S1). The staples containing the three BDT ligands surrounding the vertex Ag atom of the cluster form a concave cavity suitable for embracing the convex  $\pi$ -surface of C<sub>60</sub><sup>51,52</sup> (Figure 4B), with  $\pi$ – $\pi$  interactions being the major promoting forces behind such host–guest complexation. The magnitude of the calculated binding energy (–16.77 kcal/mol) also confirms the contribution of the vdW interaction in the system. The fullerene is clasped in the bowl of the three BDT ligands but slightly off-center from the C<sub>3</sub> axis of the cluster passing through the vertex Ag atom and the center of the icosahedron. Hence, the interaction of the fullerene with the three BDT ligands surrounding the vertex position is not similar. The interaction is stronger with the closest contacts of 3.73 and 3.85 Å for two BDT ligands (marked as “L<sub>1</sub>” and “L<sub>2</sub>” in Figure 4) than the other ligand (marked as “L<sub>3</sub>”) lying at a distance of 4.19 Å.

Here, the stabilization of the cluster, [Ag<sub>29</sub>(BDT)<sub>12</sub>]<sup>3-</sup>, by the fullerene interacting at the vertex takes place in two ways. Initially, C<sub>60</sub> is captured by the benzene rings of BDT ligands through  $\pi$ – $\pi$  interactions. Later, C<sub>60</sub> stabilizes the unpassivated Ag atom by  $\eta^2$  interaction at a 6–5 bond of the fullerene.<sup>53–55</sup>

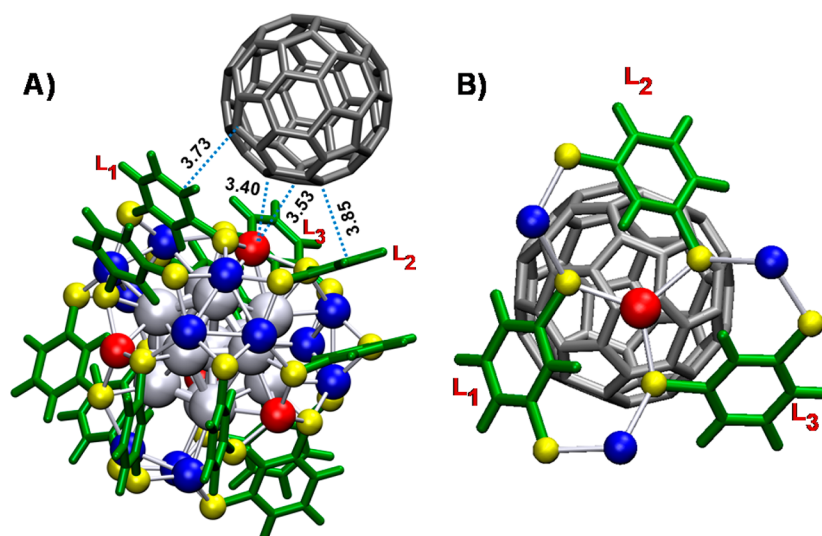


**Figure 4.** (A) DFT-optimized lowest energy structure of  $[\text{Ag}_{29}(\text{BDT})_{12}(\text{C}_{60})]^{3-}$  in which a fullerene interacts at a vertex position of the cluster. (B) Enlarged view of the staples around the vertex Ag atom showing how the three BDT ligands partially embrace the curved  $\pi$ -surface of  $\text{C}_{60}$ . The bond distances are in Å.

This is favored by ionic and vdW interactions formed between the positive charge accumulation on the Ag atom and the negative charge density localized on the 6–5 bonds of the fullerene, located at a distance of 3.40–3.53 Å from the Ag atom. The calculated Bader charges on the silver atom, Ag (+0.3080e) and on the carbon atoms of the 6–5 bond of fullerene (−0.0032e and −0.0170e) indicate weak ionic interactions. The total changes in Bader charges, including vacuum corrections on the individual molecules  $[\text{Ag}_{29}(\text{BDT})_{12}]^{3-}$  and  $\text{C}_{60}$  when these were in contact, were 0.35e and −0.50e, respectively, and this indicates that  $\text{C}_{60}$  acts as an electron acceptor and acquires a net charge of −0.15e from  $[\text{Ag}_{29}(\text{BDT})_{12}]^{3-}$ , and this imparts a partial ionic bonding in the adduct. This electron transfer also explains the chemical shift observed in the NMR measurements.

As the intermolecular interactions between the cluster and the fullerene were mainly dominated by the supramolecular effects, we also incorporated vdW correction in DFT. The lowest energy structure predicted by the vdW-DF2 functional (Figure S10) suggests slight changes in the orientation of fullerene as compared to the structure obtained by the PBE functional and allows closer contacts at a distance of 3.56 Å with the two BDT ligands and 3.67 Å with the third one. The relative contributions of  $\pi$ – $\pi$  interactions between the aromatic ligands and the fullerene versus electrostatic interactions between the fullerene and the Ag core depend on various factors such as the specific binding geometry, binding site, number of fullerenes, the size, and type of ligands. We carried out a computational study of the ligand binding energy in the case of the lowest energy isomer of  $[\text{Ag}_{29}(\text{BDT})_{12}(\text{C}_{60})]^{3-}$  (where  $\text{C}_{60}$  was attached at a tetrahedral vertex position) and found that 60% of the binding energy arises from the  $\pi$ – $\pi$  interactions. The remaining 40% arises from binding interactions of the metal core and surface  $\text{AgS}_3$  motif with  $\text{C}_{60}$  through weak ionic forces and associated van der Waals interactions. Binding at this vertex site would be most affected by the aromaticity of the ligands due to the proximity of the fullerene to the ligands. It may be assumed in this case that a smaller ligand than BDT might permit the  $\text{C}_{60}$  to come closer at the vertex site and possibly increase the ionic binding to the

$\text{AgS}_3$  motif. Complete computational details used for calculating the relative contributions of binding energy have been presented in the Supporting Information (Figure S11). The structure of  $[\text{Ag}_{29}(\text{BDT})_{12}(\text{C}_{60})]^{3-}$  was also optimized using the finite difference grid method of GPAW to obtain more accurate results and to verify the results from the more efficient LCAO basis method (Table S1).

We searched possibilities of other configurational isomers of  $[\text{Ag}_{29}(\text{BDT})_{12}(\text{C}_{60})]^{3-}$  in DFT by attaching  $\text{C}_{60}$  at the tetrahedrally oriented trigonal faces in the exterior shell of the cluster as the three partially exposed silver atoms at each of these faces may also exhibit some reactivity (Table S2). Though the calculated binding energy (−15.63 kcal/mol) indicates the possibility of some interaction, this was weaker compared to the interaction at the vertex position (−16.77 kcal/mol). We found that a  $\text{C}_{60}$  interacting at this position is at a distance of 3.54–3.81 Å from the Ag atoms, which is larger than the distance of 3.40–3.53 Å of a  $\text{C}_{60}$  at the vertex site, and the position lacks the  $\pi$ – $\pi$  interaction as the benzene rings of the BDT ligands are far away (Figure S12). DFT calculations show that binding of  $\text{C}_{60}$  at the vertex position of the cluster is the lowest energy isomer.

**Molecular Docking of  $[\text{Ag}_{29}(\text{BDT})_{12}]^{3-}$  with  $\text{C}_{60}$ .** To verify our lowest energy structure of  $[\text{Ag}_{29}(\text{BDT})_{12}(\text{C}_{60})]^{3-}$  obtained from the DFT studies based on the assumption that fullerenes would be seated in the tetrahedral symmetry positions, we further carried out a global structure search by molecular docking simulations using AutoDock4.2 and its associated software<sup>56</sup> to confirm the global minimum energy geometry of a cluster and a fullerene in close proximity. This approach was used as a complete search over all the relevant rotational, and translational degrees of freedom of the fullerene with respect to the cluster was unfeasible in DFT due to the computational cost. We used  $\text{C}_{60}$  (or  $\text{C}_{70}$ ) as the “ligand”, that is, the movable molecule. The “receptor” molecule was  $[\text{Ag}_{29}(\text{BDT})_{12}]^{3-}$ , and this was the fixed and completely rigid central molecule. For simplification, we did not use any torsion and charge parameters for the fullerene ligands. Bader charges from the optimized structures obtained in GPAW were used for all the atoms of  $[\text{Ag}_{29}(\text{BDT})_{12}]^{3-}$ .

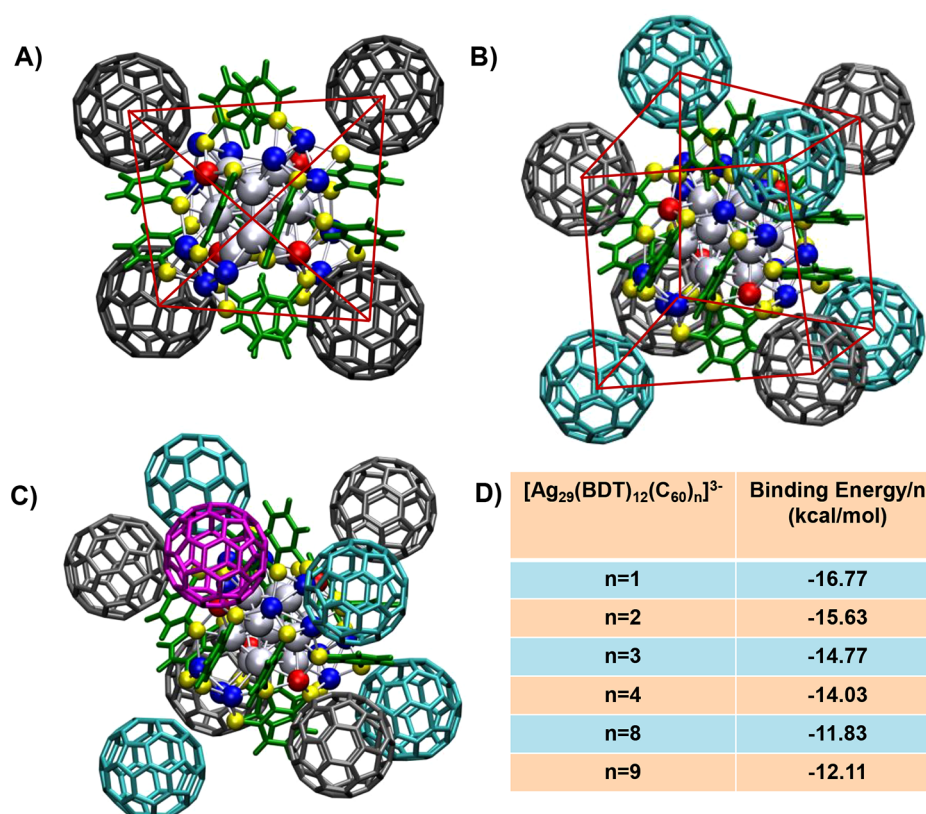


**Figure 5.** DFT-optimized lowest energy structures of (A)  $[\text{Ag}_{29}(\text{BDT})_{12}(\text{C}_{60})_4]^{3-}$ , (B)  $[\text{Ag}_{29}(\text{BDT})_{12}(\text{C}_{60})_8]^{3-}$ , and (C)  $[\text{Ag}_{29}(\text{BDT})_{12}(\text{C}_{60})_9]^{3-}$ . Color codes:  $\text{C}_{60}$  at vertex position are black, at faces are cyan, and additional fullerene placed between the face and vertex in the case of  $[\text{Ag}_{29}(\text{BDT})_{12}(\text{C}_{60})_9]^{3-}$  is purple. (D) Table showing binding energy of the complexes.

The structure showing the lowest binding energy ( $-10.29$  kcal/mol) in the docking study is shown in Figure S13. It shows that  $\text{C}_{60}$  binds at the vertex position, and this further verifies that this position is the lowest energy site for attachment of a fullerene to the cluster.

The structure of this force-field global minimum geometry (FFGMG) of the adduct obtained from the docking studies has the  $\text{C}_{60}$  shifted further toward two of the BDT ligands and offset to a greater degree from the  $\text{C}_3$  axis passing through the center of the icosahedron and the vertex Ag atom. When the FFGMG of the adduct was used as an initial structure for DFT optimization (Figure S14), it showed a slightly higher binding energy ( $-16.37$  kcal/mol) compared to that of our lowest energy structure ( $-16.77$  kcal/mol) obtained from DFT studies by our initial symmetry-based method. Molecular docking simulation utilizes only noncovalent interactions and does not treat charge transfer. The distance of  $\text{C}_{60}$  from the Ag atom ( $4.18$  Å) is greater in the case of the FFGMG of the adduct. Also, there is stronger  $\pi$ - $\pi$  interaction with two BDT ligands ( $3.16$  and  $3.41$  Å) and no interaction with the third ligand (distance  $>5.89$  Å) in the case of the molecular docking simulation (Figure S13). These changes may be attributed to the energy differences observed in the DFT optimization of the FFGMG of the adduct compared to our initial DFT-optimized lowest energy structure. Hence, electronic charge transfer effects and weak bonding with the Ag atom also contribute substantially to the binding. Also due to the rigid ligand and the receptor, additional structural relaxations on the cluster and fullerene were forbidden in the force-field docking studies, which might contribute to lowering the total energy in DFT.

#### Structures of $[\text{Ag}_{29}(\text{BDT})_{12}(\text{C}_{60})_n]^{3-}$ ( $n = 2-4, 8, \text{ and } 9$ ).

To reduce the computational cost, the structures of the other higher complexes,  $[\text{Ag}_{29}(\text{BDT})_{12}(\text{C}_{60})_n]^{3-}$  ( $n > 1$ ) were optimized only by using the PBE functional without vdW corrections, and some simplified results are presented (Table S3). Figure 5A shows the lowest energy optimized structure of  $[\text{Ag}_{29}(\text{BDT})_{12}(\text{C}_{60})_4]^{3-}$ , where the  $\text{C}_{60}$  molecules are attached at all four vertices. The structure is tetrahedral (see the 3D view in supplementary Video V2), and the fullerenes are well separated with no additional fullerene-fullerene interactions. Here, the preferred orientation of the 6-5 bond of  $\text{C}_{60}$  was preserved as in the case of  $n = 1$  for all the positions. In contrast, the lowest energy structures in the case of  $n = 2$  and 3 (Figure S15) preferred some other orientations of  $\text{C}_{60}$ . We could not find any systematic trend in the orientation of the fullerenes as a function of their number. This could be due to a change in overall symmetry of the structures that affect the overall electron delocalization. In all cases, the interaction was weak and the energy difference between the different orientations of  $\text{C}_{60}$  interacting at a particular site was very narrow, which suggests the possibility of isomerism in the complexes due to the rotation of fullerene molecules.

Experiments showed the attachment of  $n > 4$   $\text{C}_{60}$  to the cluster when reacted with an excess concentration of  $\text{C}_{60}$ . After all the tetrahedral vertex positions are occupied by the fullerenes, additional fullerenes may attach at the four tetrahedrally oriented trigonal faces formed by the 12 Ag atoms in the exterior shell. The calculated binding energy ( $-15.63$  kcal/mol) for  $\text{C}_{60}$  attaching at this position (Figure S12) supports such possibilities. Figure 5B shows the optimized structure of  $[\text{Ag}_{29}(\text{BDT})_{12}(\text{C}_{60})_8]^{3-}$ , where all the tetrahedral

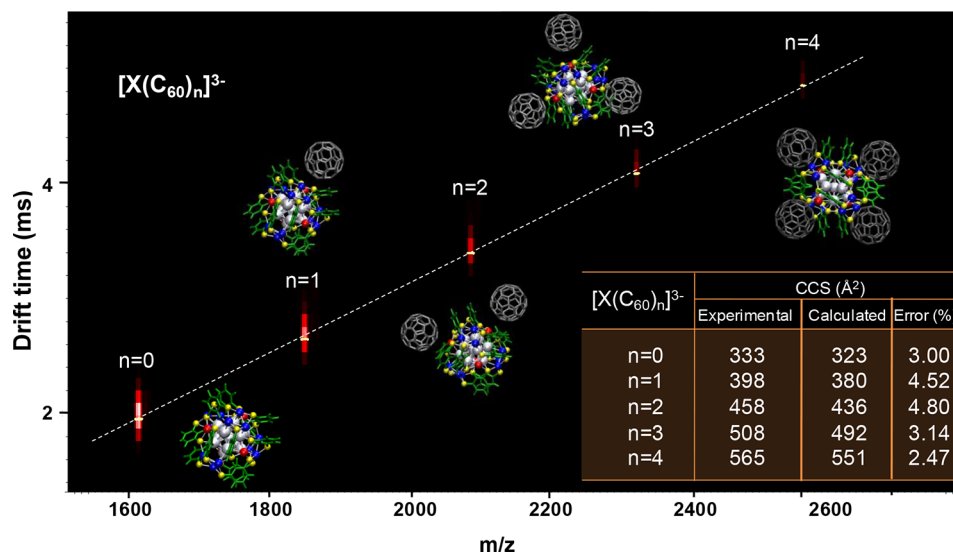


**Figure 6.** Plot of drift time of the complexes with their  $m/z$  values. Lowest energy structures of the species are shown beside their respective spots. Table in the inset of the figure shows the experimental and calculated CCS values.

vertex and face positions are occupied by  $C_{60}$  molecules. The overall geometry of  $[Ag_{29}(BDT)_{12}(C_{60})_8]^{3-}$  resembles a distorted cube (see the 3D view in [supporting Video V3](#)). The distortion is because of the nature of the asymmetric  $\pi$ - $\pi$  interaction of the BDT ligands. The length of the cube (indicated in [Figure S16](#)) is in the range of 12–15 Å, which is comparable to the lattice parameter (14.13 Å) of the face-centered cubic lattice of  $C_{60}$ .<sup>57</sup>

Experiments show that an even greater number than eight attachments of  $C_{60}$  to the cluster is possible. The structure of  $[Ag_{29}(BDT)_{12}(C_{60})_9]^{3-}$  was constructed by adding another  $C_{60}$  facing the surface of  $[Ag_{29}(BDT)_{12}(C_{60})_8]^{3-}$ , between two  $C_{60}$  molecules located at a vertex and a face, as shown in [Figure 5C](#). The interaction of the ninth  $C_{60}$  was stronger in this position compared to other locations due to three different interactions. First, it introduces fullerene–fullerene  $\pi$ - $\pi$  interaction at a distance in the range of 3.18–3.42 Å. Further, it has  $\pi$ - $\pi$  interaction with one of the BDT ligands and interaction with one of the Ag atoms at the face. The calculated binding energies of the lowest energy structures of the adducts ( $[Ag_{29}(BDT)_{12}(C_{60})_n]^{3-}$  ( $n = 1-4, 8, \text{ and } 9$ )) are listed in the table shown in [Figure 5D](#). The binding energy is found to decrease in magnitude with an increase in the number of  $C_{60}$  attachments due to the decrease in electrostatic interactions. As the number of fullerenes increases, more charge is transferred and the partial charges on the cluster decrease. This decreases the strength of the weak ionic interactions of the metal core and surface motif atoms with each fullerene, and thus the binding energy per fullerene decreases in magnitude. In the case of attachment of the ninth  $C_{60}$ , the binding energy increases in magnitude compared to that in the case of eight fullerenes due to its slightly different position between the face and vertex sites and additional fullerene–fullerene attractive vdW and  $\pi$ - $\pi$  interactions. Some additional possibilities of attachment of the ninth  $C_{60}$  over the two BDT ligands also exist ([Figure S17](#)). The addition of further fullerenes in a similar manner will form a sphere-like layer over the surface of the cluster.

**Structural Insights from Ion Mobility Mass Spectrometry (IM MS) Studies.** We used IM MS to further confirm the structure of the complexes,  $[Ag_{29}(BDT)_{12}(C_{60})_n]^{3-}$  ( $n = 1-4$ ). [Figure 6](#) represents a 2D map showing the variation of the drift

time with the  $m/z$  of the species. While passing through a buffer gas, drift time of the molecules depends on their collision cross sections (CCSs). We calculated the CCS values of our DFT-optimized lowest energy structures using the projection approximation (PA) method with nitrogen as the buffer gas as implemented in the Mobcal program package<sup>58,59</sup> and compared them to the experimental values obtained from IM MS. The table in the inset of [Figure 6](#) shows the calculated and experimental CCS of  $[Ag_{29}(BDT)_{12}(C_{60})_n]^{3-}$  ( $n = 0-4$ ).

We further constructed several other theoretical possibilities of other configurational isomers of the complexes and calculated their CCS values by the PA method to set narrow bounds to our lowest energy structures.<sup>60</sup> [Figure S18](#) shows other less favorable structures of  $[Ag_{29}(BDT)_{12}(C_{60})_4]^{3-}$  with all  $C_{60}$  molecules attached at (a) the faces of the tetrahedrally oriented trigonal planes in the exterior shell of the cluster (CCS 580 Å<sup>2</sup>, error 2.65% greater with respect to experimental CCS), (b) crowded around one vertex site of the cluster by fullerene–fullerene interaction (CCS 516 Å<sup>2</sup>, error 8.6% less with respect to experimental CCS), and (c) over the BDT ligands (CCS 598 Å<sup>2</sup>, error 5.84% greater with respect to experimental CCS). In all cases, the error in the CCS with respect to the experimental values are larger compared to the structure with  $C_{60}$  molecules attached at the four vertices.

IM MS study did not show the presence of any other isomers, which clearly confirms that one stable structure for  $[Ag_{29}(BDT)_{12}(C_{60})_4]^{3-}$  is formed by attachment of  $C_{60}$  molecules at the vertex positions on the surface of the cluster.

**Confirmation of the  $C_{60}$  Binding Sites.** The vertex Ag atoms of the cluster are also known to be functionalized by TPP ligands in case of  $[Ag_{29}(BDT)_{12}(TPP)_4]^{3-}$ .<sup>12</sup> When TPP was added to the cluster–fullerene complexes,  $[Ag_{29}(BDT)_{12}(C_{60})_n]^{3-}$  ( $n = 1-4$ ),  $C_{60}$  molecules were immediately replaced by TPP and  $[Ag_{29}(BDT)_{12}(TPP)_n]^{3-}$  ( $n = 1-4$ ) was formed ([Figure S19](#)). This further confirmed the position of the  $C_{60}$  attachment on the cluster surface. We have also tried to exchange the TPP ligands from the  $[Ag_{29}(BDT)_{12}(TPP)_4]^{3-}$  cluster with  $C_{60}$ , but such replacement was not favorable. The formation of the Ag–P bond passivates the Ag atom to a greater extent compared to that of the fullerenes which exhibit only weak vdW and electrostatic interactions. Hence, we

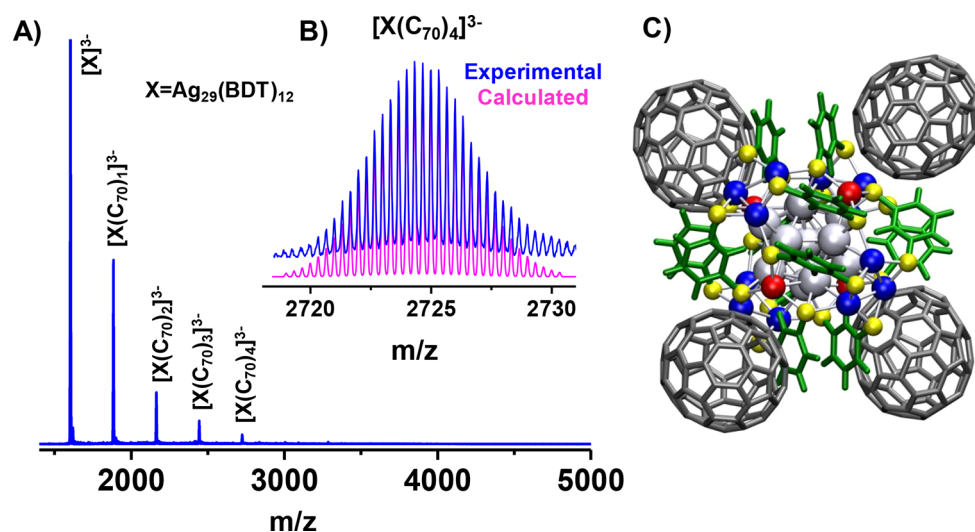


Figure 7. (A) ESI MS of  $[Ag_{29}(BDT)_{12}(C_{70})_n]^{3-}$  ( $n = 1-4$ ), (B) experimental and calculated isotope patterns of  $[Ag_{29}(BDT)_{12}(C_{70})_4]^{3-}$ , and (C) DFT-optimized lowest energy structure of  $[Ag_{29}(BDT)_{12}(C_{70})_4]^{3-}$ .

observed a competitive binding. We have also studied if there was any effect of electrostatic shielding on the binding of fullerenes. For this, salts such as NaCl, KCl, or KOAc were added to the solutions, but salts did not inhibit the binding of fullerenes (Figure S20).

**Characterization of the Complexes of C<sub>70</sub> with  $[Ag_{29}(BDT)_{12}]^{3-}$ .** The cluster exhibited similar reactivity with another fullerene, C<sub>70</sub>. At an optimum cluster/C<sub>70</sub> molar ratio of 1:4, up to four C<sub>70</sub> attachments to the cluster were observed in ESI MS (Figure 7). As discussed in the case of C<sub>60</sub>, UV–vis studies (Figure S21), CID (Figure S22), replacement of C<sub>70</sub> with TPP (Figure S23), and higher attachments at an excess concentration of C<sub>70</sub> (Figure S24) reflected similar behavior. DFT calculations and molecular docking simulations further confirmed the formation of similar structures. Complete details are included in the Supporting Information (Figures S25–S29 and Table S4).

The DFT-optimized lowest energy structure of  $[Ag_{29}(BDT)_{12}(C_{70})]^{3-}$  (Figure S25) shows that C<sub>70</sub> lies at a distance of 3.42–3.55 Å from the vertex Ag atom, similar to that of C<sub>60</sub> (3.40–3.53 Å). However, due to its larger size, C<sub>70</sub> exhibits stronger  $\pi$ – $\pi$  binding interaction with the aromatic ligands compared to C<sub>60</sub> with a closer contact of 3.32 and 3.49 Å with the two BDT ligands. For C<sub>60</sub>, distance from two nearest BDT ligands was 3.73 and 3.85 Å, as calculated using the PBE functional. C<sub>70</sub> is similarly far from the third BDT ligand at a distance of 4.36 Å. Stronger interaction is also reflected in the binding energy value of –18.68 kcal/mol for the lowest energy structure of  $[Ag_{29}(BDT)_{12}(C_{70})]^{3-}$  compared to –16.77 kcal/mol for  $[Ag_{29}(BDT)_{12}(C_{60})]^{3-}$ . The structures of  $[Ag_{29}(BDT)_{12}(C_{70})_n]^{3-}$  ( $n = 2-4$ ) (Figure S29) were also similar to that of C<sub>60</sub>. The lowest energy structure for  $n = 4$  (BE = –15.59 kcal/mol) is presented in Figure 7B. The calculated CCS values of the DFT-optimized lowest energy structures of the complexes,  $[Ag_{29}(BDT)_{12}(C_{70})_n]^{3-}$  ( $n = 1-4$ ), also matched well with the experimental CCS obtained from the IM MS study (Figure S30). The orientational changes in C<sub>70</sub> were more significant compared to C<sub>60</sub>, and this can be attributed to the larger size and ellipsoidal shape of C<sub>70</sub>, which affects the  $\pi$ – $\pi$  and vdW interactions significantly.

## CONCLUSION

In summary, we demonstrate that adducts of fullerenes are formed with monolayer-protected clusters. The complexation was assisted due to the compatible structure of the cluster and the orientation of the ligands that form tetrahedral concave cavities at the cluster surface, compatible with the convex  $\pi$ -surface of fullerenes. DFT calculations and molecular docking simulations show that vdW and  $\pi$ – $\pi$  interactions along with some weak binding with the Ag atoms facilitated the formation of the cluster–fullerene conjugates. Although our study was centered around a detailed discussion of the interaction of fullerenes C<sub>60</sub> and C<sub>70</sub> with one specific cluster,  $[Ag_{29}(BDT)_{12}]^{3-}$ , it can be extended to other monolayer-protected clusters, as well. Creating such cluster–fullerene composites in the solid state would further expand research in this field. Such composites can be interesting materials for study not only because of their structures but also due to their properties such as electrical conductivity, photoinduced charge transfer, as well as optical and mechanical properties. They can find applications in photovoltaics, sensors, and even in medical science.

## EXPERIMENTAL SECTION

**Reagents and Materials.** All the materials except the clusters were commercially available and used without further purification. Silver nitrate (AgNO<sub>3</sub>, 99.9%) was purchased from Rankem, India. 1,3-Benzenedithiol (1,3-BDT), sodium borohydride (NaBH<sub>4</sub>), and fullerenes C<sub>60</sub> (99.5%) and C<sub>70</sub> (98%) were purchased from Sigma-Aldrich. Triphenylphosphine (TPP) was purchased from Spectrochem, India. All the solvents, dichloromethane (DCM), methanol (MeOH), ethanol (EtOH), dimethylformamide (DMF), and toluene were of the HPLC grade and were used without further distillation. Deuterated solvents DMF-*d*<sub>7</sub> and toluene-*d*<sub>8</sub>, used for NMR measurements, were purchased from Sigma-Aldrich.

**Instrumentation.** The UV–vis spectra were measured using a PerkinElmer Lambda 25 UV–vis spectrophotometer. Mass spectrometric measurements were done in a Waters Synapt G2-Si high-definition mass spectrometer. The instrument was well equipped with electrospray ionization and ion mobility separation techniques. NMR measurements were done in a Bruker 500 MHz NMR spectrometer. SEM and EDS analyses were performed in a FEI QUANTA-200 SEM. Further details of instrumentation are mentioned in the Supporting Information.

**Synthesis of  $[\text{Ag}_{29}(\text{BDT})_{12}]^{3-}$  Clusters.**  $[\text{Ag}_{29}(\text{BDT})_{12}]^{3-}$  clusters were synthesized following a reported protocol<sup>12</sup> with slight modifications. About 20 mg of  $\text{AgNO}_3$  was dissolved in a mixture of 2 mL of methanol and 10 mL of DCM. To this reaction mixture, about 13.5  $\mu\text{L}$  of the 1,3-BDT ligand was added. The mixture was stirred for about 15 min, and then about 10.5 mg of  $\text{NaBH}_4$ , dissolved in 500  $\mu\text{L}$  of ice-cold water was added. The stirring was continued under dark conditions for about 5 h. Then, the reaction mixture was centrifuged, the precipitate was discarded, and the clusters were obtained as the orange supernatant. The solution was evaporated by rotary evaporation, and the orange residue was washed with methanol and finally dissolved in DMF. The solution was characterized by UV–vis and ESI MS, which confirmed the formation of  $[\text{Ag}_{29}(\text{BDT})_{12}]^{3-}$  clusters (Figure S1). However, as the clusters were synthesized without the TPP ligands, they were stable only for a few hours.<sup>12</sup>

**Synthesis of  $[\text{Ag}_{29}(\text{BDT})_{12}(\text{C}_{60})_n]^{3-}$  Complexes.** Immediately after the synthesis of  $[\text{Ag}_{29}(\text{BDT})_{12}]^{3-}$  clusters, a solution of  $\text{C}_{60}$  (in toluene) was added to the cluster solution in DMF. The addition of fullerenes increased the stability of the clusters significantly. The reactivity was monitored using UV–vis and ESI MS studies. The addition of another fullerene,  $\text{C}_{70}$ , also showed a similar behavior.

**Computational Methods.** The interaction of the fullerenes,  $\text{C}_{60}$  and  $\text{C}_{70}$ , on the surface of the  $[\text{Ag}_{29}(\text{BDT})_{12}]^{3-}$  cluster was computationally studied using DFT with the projector-augmented wave method as implemented in GPAW<sup>47,48</sup> using the PBE functional<sup>49</sup> and DZP (double- $\zeta$  plus polarization) LCAO basis set. We searched structures in DFT by attaching  $\text{C}_{60}/\text{C}_{70}$  at possible locations (tetrahedral sites) on the cluster surface considering geometrical compatibility and stabilization by the supramolecular forces. After identifying the most favorable binding site, we generated the structures of  $[\text{Ag}_{29}(\text{BDT})_{12}(\text{C}_{60})_n]^{3-}$  ( $n = 1-4, 8, \text{ and } 9$ ) based on symmetry considerations, and the structures were optimized in DFT. The orientation of fullerenes at the cluster surface (to facilitate interaction with hexagonal ( $\text{C}_6$ ) face, pentagonal ( $\text{C}_5$ ) face, 6–6 bond, and 6–5 bond) was varied to search the lowest energy conformers of the adducts. In addition, we verified the lowest energy structure of  $[\text{Ag}_{29}(\text{BDT})_{12}(\text{C}_{60})]^{3-}$  by molecular docking simulations using AutoDock4.2 and its associated software<sup>56</sup> to confirm the global minimum energy geometry of a cluster and a fullerene in close proximity, subject to some constraints, which we then optimized in DFT and compared the energy and geometry with our initial DFT-optimized lowest energy structure. Furthermore, in some cases, we optimized the structures using the finite-difference method in GPAW and also by using a van der Waals functional. The CCS of the DFT-optimized structures was calculated with the PA with nitrogen as the buffer gas as implemented in the Mobcal program package.<sup>58,59</sup> Complete computational details are included in the Supporting Information.

## ASSOCIATED CONTENT

### Supporting Information

The Supporting Information is available free of charge on the ACS Publications website at DOI: 10.1021/acsnano.7b07759.

Instrumentation, computational methods, optical absorption studies, additional ESI MS for the characterization of the cluster-fullerene adducts, and complete computational details for all possible isomers of the complexes (PDF)

Video V1: 3D view of the structure of  $[\text{Ag}_{29}(\text{BDT})_{12}]^{3-}$  (MPG)

Video V2: 3D view of the structure of  $[\text{Ag}_{29}(\text{BDT})_{12}(\text{C}_{60})_4]^{3-}$  (MPG)

Video V3: 3D view of the structure of  $[\text{Ag}_{29}(\text{BDT})_{12}(\text{C}_{60})_8]^{3-}$  (MPG)

## AUTHOR INFORMATION

### Corresponding Author

\*E-mail: pradeep@iitm.ac.in.

### ORCID

Thalappil Pradeep: 0000-0003-3174-534X

### Author Contributions

P.C. synthesized the clusters, designed and conducted all experiments. P.C. and A.N. carried out the ESI MS measurements, G.P. carried out the DFT calculations, A.N. and G.N. carried out the molecular docking simulations. The computational part was supervised by G.N., and the whole project was supervised by T.P. The manuscript was written through contributions of all authors.

### Notes

The authors declare no competing financial interest.

## ACKNOWLEDGMENTS

P.C. thanks the Council of Scientific and Industrial Research (CSIR) for a research fellowship. A.N. thanks IIT Madras for an Institute Doctoral fellowship. G.P. thanks IIT Madras for an Institute Postdoctoral fellowship. We thank the Department of Science and Technology, Government of India, for continuous support of our research program.

## REFERENCES

- Chakraborty, I.; Pradeep, T. Atomically Precise Clusters of Noble Metals: Emerging Link between Atoms and Nanoparticles. *Chem. Rev.* **2017**, *117*, 8208–8271.
- Jin, R.; Zeng, C.; Zhou, M.; Chen, Y. Atomically Precise Colloidal Metal Nanoclusters and Nanoparticles: Fundamentals and Opportunities. *Chem. Rev.* **2016**, *116*, 10346–10413.
- Mathew, A.; Pradeep, T. Noble Metal Clusters: Applications in Energy, Environment, and Biology. *Part. Part. Syst. Char.* **2014**, *31*, 1017–1053.
- Fang, J.; Zhang, B.; Yao, Q.; Yang, Y.; Xie, J.; Yan, N. Recent Advances in the Synthesis and Catalytic Applications of Ligand-Protected, Atomically Precise Metal Nanoclusters. *Coord. Chem. Rev.* **2016**, *322*, 1–29.
- Heaven, M. W.; Dass, A.; White, P. S.; Holt, K. M.; Murray, R. W. Crystal Structure of the Gold Nanoparticle  $[\text{N}(\text{C}_8\text{H}_{17})_4]_4\text{Au}_{25}(\text{SCH}_2\text{CH}_2\text{Ph})_{18}$ . *J. Am. Chem. Soc.* **2008**, *130*, 3754–3755.
- Zhu, M.; Aikens, C. M.; Hollander, F. J.; Schatz, G. C.; Jin, R. Correlating the Crystal Structure of a Thiol-Protected  $\text{Au}_{25}$  Cluster and Optical Properties. *J. Am. Chem. Soc.* **2008**, *130*, 5883–5885.
- Lopez-Acevedo, O.; Tsunoyama, H.; Tsukuda, T.; Häkkinen, H.; Aikens, C. M. Chirality and Electronic Structure of the Thiolate-Protected  $\text{Au}_{38}$  Nanocluster. *J. Am. Chem. Soc.* **2010**, *132*, 8210–8218.
- Jadzinsky, P. D.; Calero, G.; Ackerson, C. J.; Bushnell, D. A.; Kornberg, R. D. Structure of a Thiol Monolayer-Protected Gold Nanoparticle at 1.1 Å Resolution. *Science* **2007**, *318*, 430–433.
- Joshi, C. P.; Bootharaju, M. S.; Alhilaly, M. J.; Bakr, O. M.  $[\text{Ag}_{25}(\text{SR})_{18}]^-$ : The “Golden” Silver Nanoparticle. *J. Am. Chem. Soc.* **2015**, *137*, 11578–11581.
- Yang, H.; Wang, Y.; Huang, H.; Gell, L.; Lehtovaara, L.; Malola, S.; Häkkinen, H.; Zheng, N. All-Thiol-Stabilized  $\text{Ag}_{44}$  and  $\text{Au}_{12}\text{Ag}_{32}$  Nanoparticles with Single-Crystal Structures. *Nat. Commun.* **2013**, *4*, 2422.
- Desireddy, A.; Conn, B. E.; Guo, J.; Yoon, B.; Barnett, R. N.; Monahan, B. M.; Kirschbaum, K.; Griffith, W. P.; Whetten, R. L.; Landman, U.; Bigioni, T. P. Ultrastable Silver Nanoparticles. *Nature* **2013**, *501*, 399–402.
- AbdulHalim, L. G.; Bootharaju, M. S.; Tang, Q.; Del Gobbo, S.; AbdulHalim, R. G.; Eddaoudi, M.; Jiang, D.-e.; Bakr, O. M.  $[\text{Ag}_{29}(\text{BDT})_{12}(\text{TPP})_4]^-$ : A Tetravalent Nanocluster. *J. Am. Chem. Soc.* **2015**, *137*, 11970–11975.

- (13) Lu, Y.; Chen, W. Application of Mass Spectrometry in the Synthesis and Characterization of Metal Nanoclusters. *Anal. Chem.* **2015**, *87*, 10659–10667.
- (14) Harkness, K. M.; Cliffl, D. E.; McLean, J. A. Characterization of Thiolate-Protected Gold Nanoparticles by Mass Spectrometry. *Analyt Chem.* **2010**, *135*, 868–874.
- (15) Weerawardene, K. L. D. M.; Aikens, C. M. Theoretical Insights into the Origin of Photoluminescence of  $\text{Au}_{25}(\text{SR})_{18}^-$  Nanoparticles. *J. Am. Chem. Soc.* **2016**, *138*, 11202–11210.
- (16) Dou, X.; Yuan, X.; Yu, Y.; Luo, Z.; Yao, Q.; Leong, D. T.; Xie, J. Lighting up Thiolated Au@Ag Nanoclusters via Aggregation-Induced Emission. *Nanoscale* **2014**, *6*, 157–161.
- (17) Mathew, A.; Natarajan, G.; Lehtovaara, L.; Häkkinen, H.; Kumar, R. M.; Subramanian, V.; Jaleel, A.; Pradeep, T. Supramolecular Functionalization and Concomitant Enhancement in Properties of  $\text{Au}_{25}$  Clusters. *ACS Nano* **2014**, *8*, 139–152.
- (18) Martin, N.; Nierengarten, J. F. *Supramolecular Chemistry of Fullerenes and Carbon Nanotubes*; Wiley-VCH, 2012; p 403.
- (19) Tashiro, K.; Aida, T. Metalloporphyrin Hosts for Supramolecular Chemistry of Fullerenes. *Chem. Soc. Rev.* **2007**, *36*, 189–197.
- (20) Diederich, F.; Gomez-Lopez, M. Supramolecular Fullerene Chemistry. *Chem. Soc. Rev.* **1999**, *28*, 263–277.
- (21) Schuster, D. I.; Li, K.; Guldi, D. M.; Ramey, J. Novel Porphyrin-Fullerene Assemblies: from Rotaxanes to Catenanes. *Org. Lett.* **2004**, *6*, 1919–1922.
- (22) Haino, T.; Yanase, M.; Fukazawa, Y. Crystalline Supramolecular Complexes of  $\text{C}_{60}$  with Calix[5]arenes. *Tetrahedron Lett.* **1997**, *38*, 3739–3742.
- (23) Murthy, C. N.; Geckeler, K. E. The Water-Soluble  $[\beta]$ -Cyclodextrin- $[\text{C}_{60}]$  Fullerene Complex. *Chem. Commun.* **2001**, 1194–1195.
- (24) Fileti, E.; Colherinhas, G.; Malaspina, T. Predicting the Properties of a New Class of Host-Guest Complexes:  $\text{C}_{60}$  Fullerene and CB[9] Cucurbituril. *Phys. Chem. Chem. Phys.* **2014**, *16*, 22823–22829.
- (25) Moreira, L.; Calbo, J.; Krick Calderon, R. M.; Santos, J.; Illescas, B. M.; Arago, J.; Nierengarten, J. F.; Guldi, D. M.; Orti, E.; Martin, N. Unveiling the Nature of Supramolecular Crown Ether- $\text{C}_{60}$  Interactions. *Chem. Sci.* **2015**, *6*, 4426–4432.
- (26) Boyd, P. D. W.; Hodgson, M. C.; Rickard, C. E. F.; Oliver, A. G.; Chaker, L.; Brothers, P. J.; Bolskar, R. D.; Tham, F. S.; Reed, C. A. Selective Supramolecular Porphyrin/Fullerene Interactions. *J. Am. Chem. Soc.* **1999**, *121*, 10487–10495.
- (27) Sun, D.; Tham, F. S.; Reed, C. A.; Chaker, L.; Boyd, P. D. W. Supramolecular Fullerene-Porphyrin Chemistry. Fullerene Complexation by Metalated “Jaws Porphyrin” Hosts. *J. Am. Chem. Soc.* **2002**, *124*, 6604–6612.
- (28) Wang, Y.-B.; Lin, Z. Supramolecular Interactions between Fullerenes and Porphyrins. *J. Am. Chem. Soc.* **2003**, *125*, 6072–6073.
- (29) Yamamura, M.; Hongo, D.; Nabeshima, T. Twofold Fused Concave Hosts Containing Two Phosphorus Atoms: Modules for the Sandwich-Type Encapsulation of Fullerenes in Variable Cavities. *Chem. Sci.* **2015**, *6*, 6373–6378.
- (30) Sun, D.; Tham, F. S.; Reed, C. A.; Chaker, L.; Burgess, M.; Boyd, P. D. W. Porphyrin–Fullerene Host–Guest Chemistry. *J. Am. Chem. Soc.* **2000**, *122*, 10704–10705.
- (31) Haddon, R. C. Electronic structure, Conductivity and Superconductivity of Alkali Metal Doped  $\text{C}_{60}$ . *Acc. Chem. Res.* **1992**, *25*, 127–33.
- (32) Stephens, P. W.; Mihaly, L.; Lee, P. L.; Whetten, R. L.; Huang, S.-M.; Kaner, R.; Diederich, F.; Holczer, K. Structure of Single-Phase Superconducting  $\text{K}_3\text{C}_{60}$ . *Nature* **1991**, *351*, 632–634.
- (33) Rosseinsky, M. J.; Ramirez, A. P.; Glarum, S. H.; Murphy, D. W.; Haddon, R. C.; Hebard, A. F.; Palstra, T. T. M.; Kortan, A. R.; Zahurak, S. M.; Makhija, A. V. Superconductivity at 28 K in  $\text{Rb}_x\text{C}_{60}$ . *Phys. Rev. Lett.* **1991**, *66*, 2830–2832.
- (34) Hebard, A. F.; Rosseinsky, M. J.; Haddon, R. C.; Murphy, D. W.; Glarum, S. H.; Palstra, T. T. M.; Ramirez, A. P.; Kortan, A. R. Superconductivity at 18 K in Potassium-Doped  $\text{C}_{60}$ . *Nature* **1991**, *350*, 600–601.
- (35) Holczer, K.; Klein, O.; Huang, S.-m.; Kaner, R. B.; Fu, K. J.; Whetten, R. L.; Diederich, F. Alkali-Fulleride Superconductors: Synthesis, Composition, and Diamagnetic Shielding. *Science* **1991**, *252*, 1154.
- (36) Plotniece, M.; Kampars, V. Review: Novel Donor-Acceptor Systems of Tetrathiafulvalenes-Fullerene  $\text{C}_{60}$  (TTF- $\text{C}_{60}$ ). *Rigas Teh. Univ. Zinat. Raksti, Ser. 1* **2005**, *10*, 23–36.
- (37) Pradeep, T.; Singh, K. K.; Sinha, A. P. B.; Morris, D. E. A Stable Fullerene Charge-Transfer Complex in the Solid State: HMTTEF- $\text{C}_{60}$ . *J. Chem. Soc., Chem. Commun.* **1992**, 1747–1748.
- (38) Konarev, D. V.; Lyubovskaya, R. N.; Semkin, V. N.; Graja, A. Donor-Acceptor Interactions in  $\text{C}_{60}$  Complexes with Initially Planar  $\pi$ -Donors. *Mol. Cryst. Liq. Cryst. Sci. Technol., Sect. C* **1998**, *11*, 35–42.
- (39) Konarev, D. V.; Lyubovskaya, R. N.; Drichko, N. Y. V.; Yudanova, E. I.; Shul'ga, Y. M.; Litvinov, A. L.; Semkin, V. N.; Tarasov, B. P. Donor-Acceptor Complexes of Fullerene  $\text{C}_{60}$  with Organic and Organometallic Donors. *J. Mater. Chem.* **2000**, *10*, 803–818.
- (40) Konarev, D. V.; Semkin, V. N.; Graja, A.; Lyubovskaya, R. N. Steric Conditions for Donor–Acceptor Interactions in  $\text{C}_{60}$  Complexes with Planar Organic Donors. *J. Mol. Struct.* **1998**, *450*, 11–22.
- (41) Pursell, J. L.; Pursell, C. J. Host–Guest Inclusion Complexation of  $\alpha$ -Cyclodextrin and Triiodide Examined Using UV–Vis Spectrophotometry. *J. Phys. Chem. A* **2016**, *120*, 2144–2149.
- (42) Wood, J. M.; Kahr, B.; Hoke, S. H.; Dejarne, L.; Cooks, R. G.; Ben-Amotz, D. Oxygen and Methylene Adducts of  $\text{C}_{60}$  and  $\text{C}_{70}$ . *J. Am. Chem. Soc.* **1991**, *113*, 5907–5908.
- (43) Morand, K. L.; Hoke, S. H.; Eberlin, M. N.; Payne, G.; Cooks, R. G. Quadrupole Ion Trap Mass Spectrometry of Fullerenes. *Org. Mass Spectrom.* **1992**, *27*, 284–288.
- (44) Okada, H.; Komuro, T.; Sakai, T.; Matsuo, Y.; Ono, Y.; Omote, K.; Yokoo, K.; Kawachi, K.; Kasama, Y.; Ono, S.; Hatakeyama, R.; Kaneko, T.; Tobita, H. Preparation of Endohedral Fullerene Containing Lithium ( $\text{Li}@\text{C}_{60}$ ) and Isolation as Pure Hexafluorophosphate Salt ( $[\text{Li}^+@\text{C}_{60}][\text{PF}_6^-]$ ). *RSC Adv.* **2012**, *2*, 10624–10631.
- (45) Haino, T.; Yanase, M.; Fukunaga, C.; Fukazawa, Y. Fullerene Encapsulation with Calix[5]arenes. *Tetrahedron* **2006**, *62*, 2025–2035.
- (46) Anderson, T. W.; Sanders, J. K. M.; Santos, G. D. The Sergeants-and-Soldiers Effect: Chiral Amplification in Naphthalenediimide Nanotubes. *Org. Biomol. Chem.* **2010**, *8*, 4274–4280.
- (47) Mortensen, J. J.; Hansen, L. B.; Jacobsen, K. W. Real-Space Grid Implementation of the Projector Augmented Wave Method. *Phys. Rev. B: Condens. Matter Mater. Phys.* **2005**, *71*, 035109.
- (48) Enkovaara, J.; Rostgaard, C.; Mortensen, J. J.; Chen, J.; Dulak, M.; Ferrighi, L.; Gavnholt, J.; Glinsvad, C.; Haikola, V.; Hansen, H. A.; Kristoffersen, H. H.; Kuisma, M.; Larsen, A. H.; Lehtovaara, L.; Ljungberg, M.; Lopez-Acevedo, O.; Moses, P. G.; Ojanen, J.; Olsen, T.; Petzold, V.; et al. Electronic Structure Calculations with GPAW: a Real-Space Implementation of the Projector Augmented-Wave Method. *J. Phys.: Condens. Matter* **2010**, *22*, 253202.
- (49) Perdew, J. P.; Burke, K.; Ernzerhof, M. Generalized Gradient Approximation Made Simple. *Phys. Rev. Lett.* **1997**, *78*, 1396–1396.
- (50) Ishii, T.; Aizawa, N.; Yamashita, M.; Matsuzaka, H.; Kodama, T.; Kikuchi, K.; Ikemoto, I.; Iwasa, Y. First Syntheses of Cocrystallites Consisting of Anti-formed Metal Octaethylporphyrins with Fullerene  $\text{C}_{60}$ . *J. Chem. Soc., Dalton Trans.* **2000**, 4407–4412.
- (51) Filatov, A. S.; Ferguson, M. V.; Spisak, S. N.; Li, B.; Campana, C. F.; Petrukhina, M. A. Bowl-Shaped Polyarenes as Concave–Convex Shape Complementary Hosts for  $\text{C}_{60}^-$  and  $\text{C}_{70}^-$  Fullerenes. *Cryst. Growth Des.* **2014**, *14*, 756–762.
- (52) Perez, E. M.; Martin, N. Curves Ahead: Molecular Receptors for Fullerenes Based on Concave-Convex Complementarity. *Chem. Soc. Rev.* **2008**, *37*, 1512–1519.
- (53) Jayaratna, N. B.; Olmstead, M. M.; Kharisov, B. I.; Dias, H. V. R. Coinage Metal Pyrazolates  $[(3,5-(\text{CF}_3)_2\text{Pz})\text{M}]_3$  ( $\text{M} = \text{Au}, \text{Ag}, \text{Cu}$ ) as Buckycatchers. *Inorg. Chem.* **2016**, *55*, 8277–8280.

(54) Halim, M.; Kennedy, R. D.; Suzuki, M.; Khan, S. I.; Diaconescu, P. L.; Rubin, Y. Complexes of Gold(I), Silver(I), and Copper(I) with Pentaary[60]fullerides. *J. Am. Chem. Soc.* **2011**, *133*, 6841–6851.

(55) Olmstead, M. M.; Maitra, K.; Balch, A. L. Formation of a Curved Silver Nitrate Network that Conforms to the Shape of  $C_{60}$  and Encapsulates the Fullerene-Structural Characterization of  $C_{60}\{Ag-(NO_3)\}_5$ . *Angew. Chem., Int. Ed.* **1999**, *38*, 231–233.

(56) Morris, G. M.; Huey, R.; Lindstrom, W.; Sanner, M. F.; Belew, R. K.; Goodsell, D. S.; Olson, A. J. AutoDock4 and AutoDockTools4: Automated Docking with Selective Receptor Flexibility. *J. Comput. Chem.* **2009**, *30*, 2785–2791.

(57) Quo, Y.; Karasawa, N.; Goddard, W. A. Prediction of Fullerene Packing in  $C_{60}$  and  $C_{70}$  Crystals. *Nature* **1991**, *351*, 464–467.

(58) von Helden, G.; Hsu, M. T.; Gotts, N.; Bowers, M. T. Carbon Cluster Cations with up to 84 Atoms: Structures, Formation Mechanism, and Reactivity. *J. Phys. Chem.* **1993**, *97*, 8182–8192.

(59) Shvartsburg, A. A.; Jarrold, M. F. An Exact Hard-Spheres Scattering Model for the Mobilities of Polyatomic Ions. *Chem. Phys. Lett.* **1996**, *261*, 86–91.

(60) Greisch, J. F.; Amsharov, K. Y.; Weippert, J.; Weis, P.; Böttcher, A.; Kappes, M. M. From Planar to Cage in 15 Easy Steps: Resolving the  $C_{60}H_{21}F_9^- \rightarrow C_{60}^-$  Transformation by Ion Mobility Mass Spectrometry. *J. Am. Chem. Soc.* **2016**, *138*, 11254–11263.